We are IntechOpen,
the world's leading publisher of
Open Access books
Built by scientists, for scientists

4,800
Open access books available

122,000
International authors and editors

135M
Downloads

Our authors are among the

154
Countries delivered to

TOP 1%
most cited scientists

12.2%
Contributors from top 500 universities

CLARIVATE ANALYTICS
BOOK CITATION INDEX
INDEXED

WEB OF SCIENCE™

Selection of our books indexed in the Book Citation Index
in Web of Science™ Core Collection (BKCI)

Interested in publishing with us?
Contact book.department@intechopen.com

Numbers displayed above are based on latest data collected.
For more information visit www.intechopen.com

A Fluorine-Free Oxalate Route for the Chemical Solution Deposition of YBa$_2$Cu$_3$O$_7$ Films

Luis De Los Santos Valladares, Juan Carlos González,
Angel Bustamante Domínguez, Ana Maria Osorio Anaya,
Henry Sanchez Cornejo, Stuart Holmes, J. Albino Aguiar and
Crispin H.W. Barnes

Additional information is available at the end of the chapter

http://dx.doi.org/10.5772/59359

1. Introduction

To date there has been intensive research, both theoretical and experimental, about epitaxial growth of high critical temperature superconductor (HTS) thin films [1, 2]. The term epitaxy (from the Greek roots *epi*, meaning "above", and *taxis*, meaning "order") appeared around 50 years ago and refers to the growth of an oriented film on a substrate which can be based on the same substrate material (homoepitaxy) or onto a different material (heteroepitaxy). YBa$_2$Cu$_3$O$_7$ (YBCO) is one most studied HTS [3,4]. It has an orthorhombic structure and it is superconductor below the critical temperature (T_C) around 90 K. The superconductivity mechanism in this material is related to the presence of CuO$_2$ planes and charge carriers reservoir planes in its crystalline structure [5]. The interest in developing superconducting YBCO films is to produce second generation superconducting tapes [6] which, under the absence of magnetic fields, can transport high electric current densities (~10^6 A/cm^2) at liquid nitrogen temperature (77 K).

To achieve the epitaxial growth, the crystal lattice of the substrate must match with that of YBCO, permitting a small difference between them (e.g. $a_{substrate}$ ~ 3.9 Å, a_{YBCO} ~ 3.8 Å). If the lattice constant of the substrate differs from that of YBCO, the epitaxial growth is not achieved, resulting in a small amount of grains oriented in the *c*-axis and hence in anisotropy of the critical current density and magnetic susceptibility.

The methods for synthesizing YBCO layers can be classified into two categories: in-situ and ex-situ. In the in-situ methods, the YBCO phase is formed during deposition. Some of them are:

Pulsed laser deposition (PLD), liquid phase epitaxy (LPE) and metal organic chemical vapour deposition (MOCVD) [7-13]. In the ex-situ methods, the nucleation and growth of the YBCO film takes place after the deposition, by subsequent heat treatments [14,15]. The advantage of the in-situ techniques over the ex-situ ones are that they allow YBCO films with high J_C values, they can control thickness of the film and they can permit partially substitution of rare-earth elements during growing. Nevertheless, these techniques require sophisticated apparatus and high vacuum systems which make the technique expensive for commercial purposes. In contrast, the ex-situ techniques, in particular the Chemical Solution Deposition (CSD), are more attractive since they are cheap, fast and can provide large areas films and mass production. In this chapter, a fluorine-free CSD method is introduced for the fabrication of YBCO films on different substrates.

2. Chemical solution deposition technique for obtaining YBCO films

Chemical solution deposition is an ex-situ technique in which a chemical solution precursor is deposited on substrates to epitaxially grow YBCO layers [16,17]. It does not require expensive conditions or equipments such as high vacuum, irradiation or sputtering. In this technique, a solution precursor containing stoichiometric cations of Y, Ba and Cu (with ratio 1: 2: 3) is prepared, usually by sol gel, and directly deposited onto single crystals or templates which transfers their texture to the coating. The YBCO textured film is then obtained after heat treatments in oxidizing atmosphere [18, 19]. Therefore, this technique is cheap, fast and can provide large-area films. In the present work, depending on the Trifluoroacetate composition of the precursor solution, the CSD is classified into two routes: Trifluoroacetate and free-trifluoroacetates.

2.1. Trifluoroacetate metal-organic CSD route

The trifluoroacetate metal-organic (TFA-MOD) CSD route is promising for producing YBCO superconducting films with high critical current density (J_C) values [20-26]. This technique was introduced by Gupta et al. in 1988 in order to prevent the formation of $BaCO_3$ of the YBCO films usually obtained by CSD [27]. In fact, in other different CSD routes, $BaCO_3$ agglomerates at the grain boundaries affecting the J_C of the YBCO textured films. However, in the TFA-MOD BaF_2 forms during the decomposition of the organic compounds (during pyrolisis) and the YBCO films are then obtained via hydrolysis of BaF_2 [28].

In this technique, the precursor solution is prepared by mixing Y and Ba trifluoroacetates with Cu acetate (in molar ratio 1:2:3) in methanol [29] or water [30]. The organic components are eliminated by pyrolisis at around 400 °C, yielding in Y_2O_3, BaF_2 and CuO. These intermediate compounds are then transformed into YBCO tetragonal (non superconductor) by annealing at around 800 °C. The reaction follows the equation [31]:

$$0.5Y_2O_3 + 2BaF_2 + 3CuO + 2H_2O \rightarrow YBa_2Cu_3O_{7-x} + 4HF\uparrow \tag{1}$$
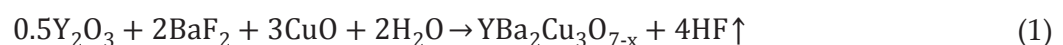
The superconducting YBCO (orthorhombic) is obtained by oxygenating the latest compound at high temperatures. Nevertheless, the release of the HF-gas product during heat treatments makes this technique hazardous for health and environment. Thus non-fluorine routes are necessary to be investigated.

2.2. Free-trifluoroacetate CSD routes

Chemical solution deposition routes which does not require the use of trifluoroacetates are vast. However, most of them result in YBCO films containing unreacted and/or secondary phases such as Y$_2$O$_3$, BaCO$_3$, Y$_2$BaCuO$_5$ (Y211), BaCuO$_2$, Cu$_2$BaO$_2$, etc. Table 1 list free-trifluoroacetates routes reported in the literature which do not require carbonate ingredients and without BaCO$_3$ formation. The routes are listed according to the employed reagents. In metal alkoxides routes the gelation rate of the precursor solution is adjusted by choosing the proper solvent. The solidification includes the hydrolysis and condensation of the alkoxides through which a polymeric product is formed [32]. However, since the rate of hydrolysis of Y and Ba are faster than that for Cu, different sized clusters results in the sol [33]. In the hydrox-ides route Ba(OH)$_2$ and Y-and Ba-trimethylacetates are reacted in propionic acid with amine solvent. Remarkably, it has been reported that this stock solution is stable in air and has a shelf life longer than 2 years [34-36]. On the other hand, the CSD based on nitrates, which is also known as polymer-assisted deposition (PAD) because of the use of polymers, obtains a homogeneous distribution of the metal precursors in the solution and the formation of uniform metal–organic films [37]. The formed NO and/or NO$_2$ can be easily eliminated leading in a high homogeneity of the precursor solution. In the following sections, a novel fluorine-free method, based on oxalates, for the CSD of YBCO films is described.

Route	Ingredients	Solvent	Substrate	Advantage	Disadvantage	Ref.
Metal alkoxides	M(OR)$_n$ where M=Y, Ba and Cu, and R=CH$_3$, CH$_2$O$_5$	H$_2$O, CH$_3$OH	Ni	It is possible to control the degree of gelation.	Inhomogeneity of the precursor gel.	[32]
Acetyl acetonates	APyP, where A= acetylacetone of Y, Ba and Cu, Py= pyridine, and P = acid	C$_5$H$_5$N, CF$_3$CO$_2$H, CH$_3$OH	MgO, YSZ	Smooth surface	Films composed of dispersed grains	[38]
Hydroxides	Y(C$_4$H$_9$COO)$_3$, Ba(OH)$_2$ and Cu- trimethyl acetate	Propionic acid / amine solvent	YSZ, LaAlO$_3$, MgO	Smooth surface without cracks	Difficult to reproduce	[34-36, 39-42]
Nitrates	Y(NO$_3$), Ba(NO$_3$) and Cu(NO$_3$)	(CH$_3$)$_2$NC(O)H	SrTiO$_3$, LaAlO$_3$	Homogeneous solution precursor	Requires rapid drying to prevent premature crystallization	[43]

Note: YSZ refers to Yttria-stabilized Zirconia (Y:ZrO$_2$)

Table 1. Classification of some free-trifluoroacetate CSD routes depending on the reagents reported in the literature and which do not result on YBCO films containing BaCO$_3$.

3. Substrates

Similar to the in-situ technique, CSD of YBCO superconducting layers also includes careful selection of substrates. To obtain high quality growth of YBCO, many considerations should be taking into mind, such as:

- The potential substrates should have lattice constant similar to that of YBCO orthorhombic so as to allow epitaxial growth.

- They must be highly insulating for eventual applications in electrical circuits.

- Ferromagnetic substrates must be discarded since they affect the diamagnetic properties of the YBCO superconducting film.

- They should have a high melting point since the fabrication of the film requires high temperatures (usually higher than 800 °C).

Some materials which meet well the requirements listed above and are: sapphire (Al_2O_3), magnesium oxide (MgO), cerium dioxide (CeO_2), yttrium oxide (Y_2O_3), lanthanum aluminate ($LaAlO_3$), strontium titanate ($SrTiO_3$) and Yttria-stabilized Zirconia ($Y:ZrO_2$, YSZ). The following sections describe the CSD of YBCO superconducting films onto the three latest substrates ($LaAlO_3$, $SrTiO_3$ and YSZ). The substrates used in this work (5 mm^2 area) were purchased from CrysTec Ltd. and their main characteristics are listed in Table 2. Note that from them, the YSZ substrate present the highest mismatch in lattice constant with respect to YBCO which, as it will be discussed below, influences in the crystallization, composition, texture and magnetic properties of the resulting YBCO film.

Material	Crystal structure	Lattice constant (nm)	Mismatch with YBCO (%)	Density at 25 °C (×10^3 kg/m^3)	Melting point (K)	Thermal expansion (K^{-1})
$LaAlO_3$	p.c.	0.3821	-0.83	6.51	2380	10×10^{-6}
$SrTiO_3$	c.p.	0.3905	+1.35	5.12	2353	9×10^{-6}
YSZ	Cubic	0.512	+32.88	5.90	2780	9.2×10^{-6}

Note: p.c: Pseudocubic (with microtwins parallel to (100)), c.p: Cubic perovskite structure.

Table 2. Some physical properties of the substrates used for the CSD of YBCO superconducting in this work.

4. Solution preparation and deposition

The first step of the CSD technique to obtain YBCO superconducting films is the preparation of the precursor solution. This solution is required to have homogeneously dispersed Y, Ba and Cu cations, suitable viscosity and without precipitation so as to achieve good adherence to the surface of the substrate and desired thickness of the resulting YBCO film.

Figure 1 provides a schematic representation of the manufacturing process of the YBCO film followed in this work. Initially a precursor solution is obtained by sol-gel similar to previous reports [44-48]. Stoichiometric amounts of yttrium, barium and copper acetates $(Y(OOCCH_3)_3.4H_2O$, $Ba(OOCCH_3)_2$ and $Cu(OOCCH_3)_2.2H_2O$ respectively) were mixed and completely dissolved in a solution of ethanol (C_2H_5OH) and oxalic acid $(H_2C_2O_4)$ (1:1 ratio). The system was left to decant for about 12 h. The matrix was then dispersed and magnetically stirred at 250 rpm to achieve a homogeneous metathesis reaction (without the segregation of any particular constituents) between the acetate solution and the oxalic acid. The resulting precursor solution was a colloid based on Y, Ba and Cu oxalates. Single drops of this precursor were carefully dripped on the $LaAlO_3(100)$, $SrTiO_3(100)$ and $YSZ(100)$ substrates with the help of a Fisher pipette. The samples were immediately dried in an oven at 40 °C. The last steps were repeated 7 times. The oxalate is formed by the reaction [49]:
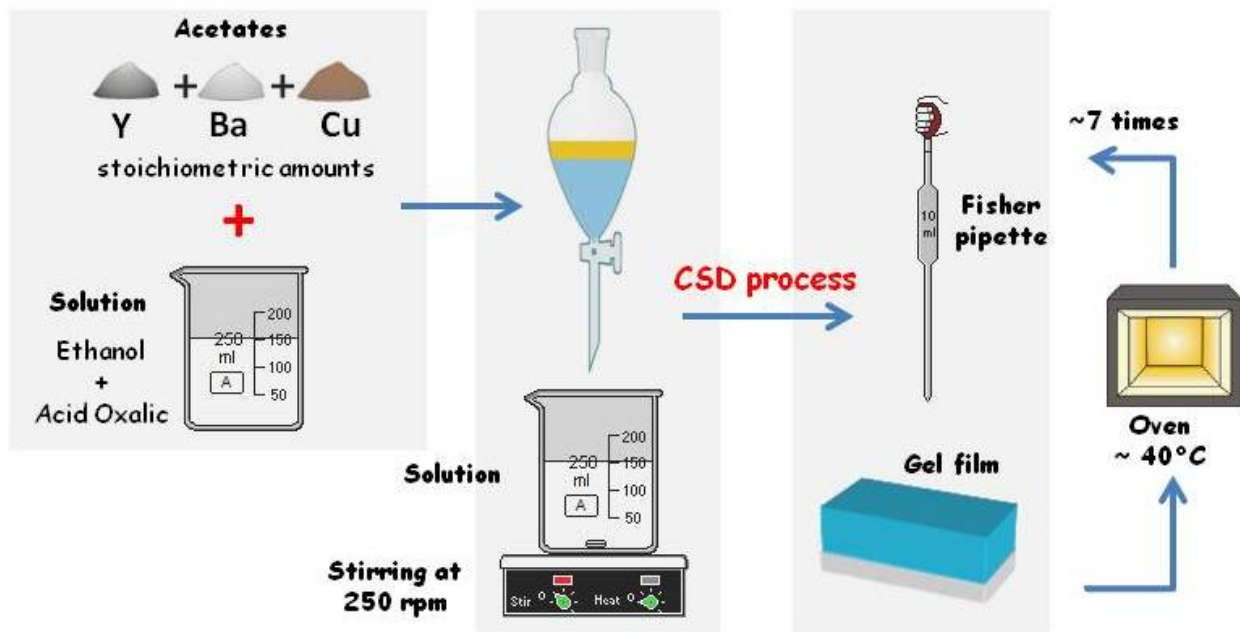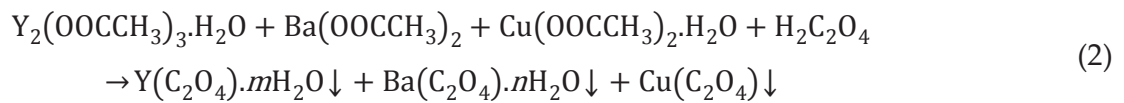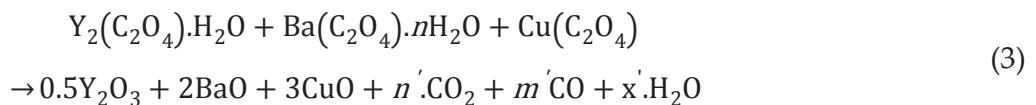
$$Y_2(OOCCH_3)_3.H_2O + Ba(OOCCH_3)_2 + Cu(OOCCH_3)_2.H_2O + H_2C_2O_4$$
$$\rightarrow Y(C_2O_4).mH_2O\downarrow + Ba(C_2O_4).nH_2O\downarrow + Cu(C_2O_4)\downarrow \tag{2}$$

Figure 1. Schematic representation followed in this work for the fabrication of YBCO superconducting films on LaA-lO₃(100), SrTiO₃(100) and YSZ(100) substrates by chemical solution deposition. Initially a precursor solution is obtained by reacting stoichiometric amounts of yttrium, barium and copper acetates in a solution of ethanol and oxalic acid (1:1 ratio). After decanting the solution for 12 h, it was dispersed by magnetic agitation to achieve a homogeneous metathesis reaction between acetate and oxalic acid. The resulting precursor solution was carefully dripped onto LaAlO₃, SrTiO₃ and YSZ substrates and they were immediately dried in an oven at 40 °C. The last two steps were repeated 7 times.
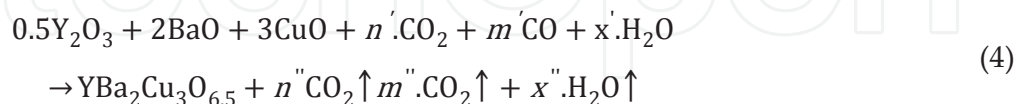
5. Heat treatments

$YBa_2Cu_3O_{7-x}$ has relatively strong oxygen-metal bonds, thus high temperatures heat treatments are required to rearrange the species in the precursor solution for a correct crystallization and crystal growth. The thermodynamic stability of YBCO limits the synthesis and the crystal growth parameters. For example synthesis at temperatures well below 900 ℃ result in x values from 0.7 to 1, leading the crystalline structure as tetragonal (non superconductor). Further oxidization at high temperatures is necessary to decrease x to ~ 0, from which cooling it below the phase transition range (~ 700 ℃ [50]) results in the orthorhombic structure (superconductor).

In this work, the crystallization and epitaxial growth of the YBCO layers were achieved by ex-situ heat treatments, as represented in Fig. 2. After drying the samples for 10 min, they were annealed at 860 °C in a tubular furnace (LENTON LTF-PTF Model 16/610) in low oxygen atmosphere for 12 h. The low oxygen atmosphere facilitates the liquid phase formation, which in turn influences the grain growth and interconnection between crystallites [51]. On the other hand, the slow heating rate (1 °C/min) permits the thermal decomposition to remove residual volatile hydrocarbons thus lowering the risk of trapping CO_2 bubbles in. Besides, it is expected that both, the slow rate and the high annealing temperature performed in this work also prevent the formation of $BaCO_3$ [52]. Thus, the chemical reaction during this process might described by [49]:

$$Y_2(C_2O_4).H_2O + Ba(C_2O_4).nH_2O + Cu(C_2O_4)$$
$$\rightarrow 0.5Y_2O_3 + 2BaO + 3CuO + n'.CO_2 + m'CO + x'.H_2O \tag{3}$$

obtaining mixtures of yttrium, barium and copper oxides (Y_2O_3, BaO and CuO). At this stage, epitaxial growth of the crystallites occurs specially at the interface of the layer/substrate, together with a considerable decrease of the thickness of the film (as it is represented in the bottom part of the figure) [53]. Furthermore, the microstructure of the film might consist of irregular arrangement of porous together with groups of chemically bounded crystallites. The reaction is described by [49]:

$$0.5Y_2O_3 + 2BaO + 3CuO + n'.CO_2 + m'CO + x'.H_2O$$
$$\rightarrow YBa_2Cu_3O_{6.5} + n''CO_2\uparrow m''.CO_2\uparrow + x''.H_2O\uparrow \tag{4}$$

Note also that at this stage the sample consists on $YBa_2Cu_3O_x$ (probably with x=6.5 [49], which is not a superconductor). The sintering of the YBCO superconducting ($YBa_2Cu_3O_7$, orthorhombic structure) is obtained after oxygenating the sample at higher temperatures than 800 ℃. For example, the represented oxygenation at 860 °C in Fig. 2 promotes the increase of the density of the layer and the epitaxial growth of the crystallites toward the surface, consuming other disoriented grains to a thermodynamically stable phase during this process. The sintering process of YBCO superconducting during oxygenation is thus described by [49]:

$$YBa_2Cu_3O_{6.5} + 0.25O_2 \rightarrow YBa_2Cu_3O_7 \qquad (5)$$
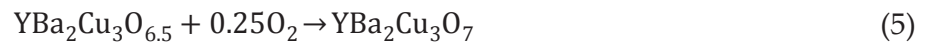
Eventually, the samples were subsequently quenched to room temperature with an intermediate step at 600 °C so as to minimise the stress in the film.
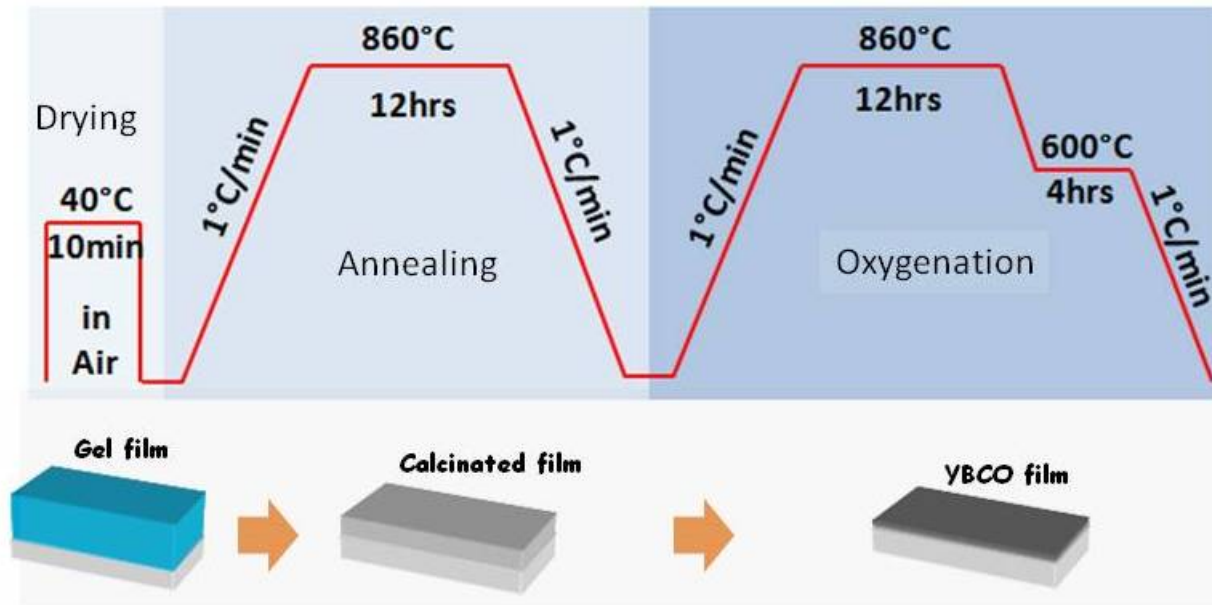

Figure 2. Schematic representation of the ex-situ heat treatments performed on CSD YBCO films. Initially the samples were dried at 40 °C for 10 min. Then they were annealed at 860 °C in oxygen flow for 12h. The slow heating rate (1 °C/min) released volatile hydrocarbons. Epitaxial growth of the crystallites occurs together with a considerably decrease of the thickness of the film. At this stage the sample consists on YBa$_2$Cu$_3$O$_x$ (with unknown x value). The sintering of the YBCO superconducting film is obtained after oxygenating the sample at 860 ℃.

6. Surface morphology

Figure 3 shows the surface morphology of the YBCO films on LaAlO$_3$, SrTiO$_3$ and YSZ substrates obtained by the oxalate CSD route and after oxygenation at three different temperatures: 820 840 and 860 °C. The results reveal that all the samples consist on granular films. In the case of the sample deposited on LaAlO$_3$ the YBCO grains are uniformly dispersed over the substrate surface, forming small groups. Previous results report that the average grain size formed is smaller than 100 nm [47]. In the case of the sample deposited on SrTiO$_3$, continuous films are clearly distinguished independently of the oxygenation temperature. However for the sample annealed at 820 °C, bright spots are spread on the surfaces. The light in the microscope might reflect in different directions when it is incident to some clusters or grains spread on the surface of the sample. Note also the formation of wide cracks (~ 5 µm) on the surface of the samples revealing parts of the underneath substrate. These cracks, which are typical for ceramic films under stress, together with some fringes formed on the surfaces (especially in the case of 860 °C annealing) suggest that the YBCO films strain during quench-

ing. The samples deposited on the YSZ substrates also present some cracks indicating stress during the quenching. However, the granular nature of the films is more pronounced than in the previous cases. On this substrate, the accumulation of grains is better appreciated in the film treated at 820 °C, whereas the surface softens at higher temperatures as it is clearly observed on the sample treated at 860 °C revealing the occurrence of melting. Furthermore, on all the samples, macro-segregation, leading to the formation of secondary phases and degradation of the epitaxy might occur as it is studied in more detail by XRD below.
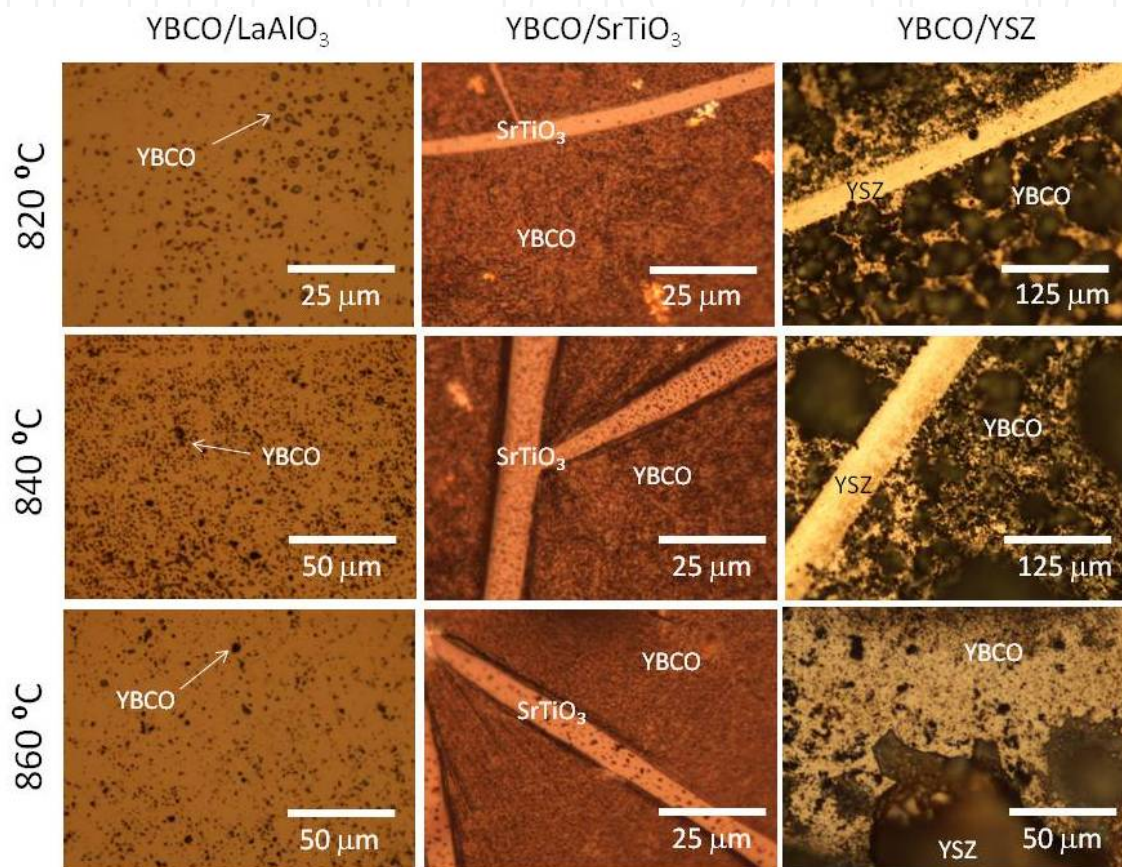

Figure 3. Optical microscopy images of the YBCO films obtained by the oxalate CSD route on LaAlO$_3$, SrTiO$_3$ and YSZ substrates after oxygenation at three different temperatures: 820, 840 and 860 °C. All the samples consist of granular films.

7. Crystallization

YBaCu$_3$O$_7$ films can grow in three different orientations: a) random, b) along the *a-b* plane and c) along the *c*-axis. In the case of YBCO films grown by the CSD technique, highly-randomly-oriented crystallites result if the fabrication has been performed without systematic control of the viscosity, homogeneity, cations ratio, etc during sol-gel and temperature, oxygen pressure, water pressure, etc during heat treatments. Fig. 4 depicts a representation of the crystallites in

an YBCO film oriented along the *a-b* plane and along the *c*-axis. For technological applications, a *c*-axis orientation growth of the YBCO film is preferable.
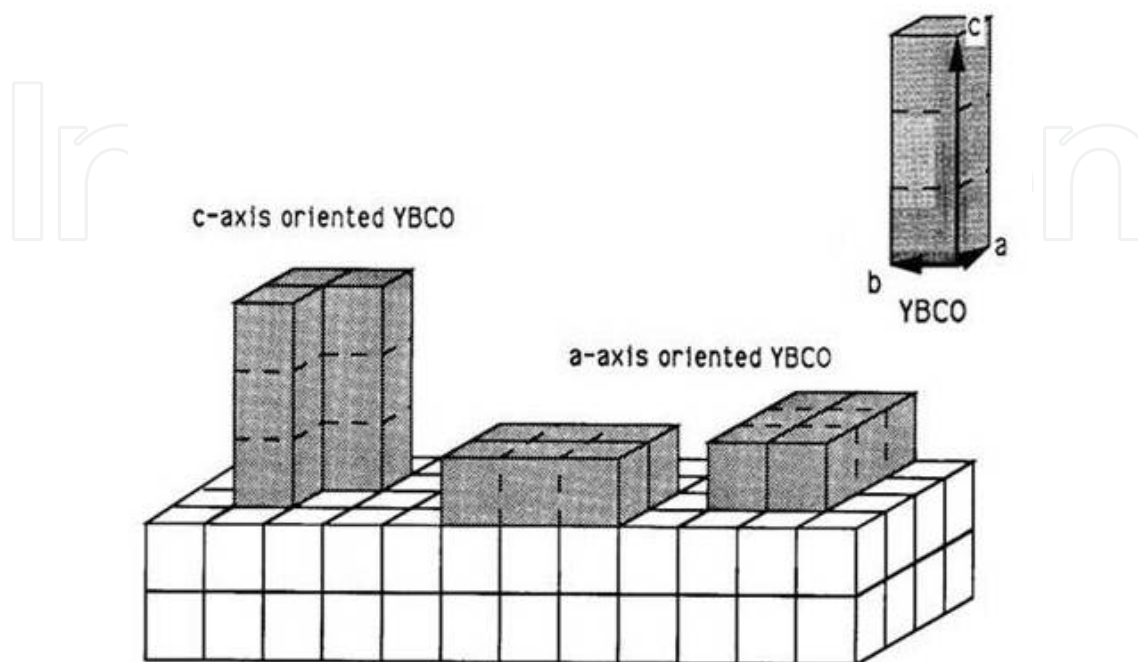

Figure 4. Schematic representation of the crystallites in an YBCO film oriented along the *a*-axis and along the *c*-axis.

The crystal orientation of YBCO thin films is commonly studied by X-ray diffraction. Fig. 5 shows the 4 representative angles (θ−2θ, ω, ϕ and Ψ) of the goniometer in a diffractometer. In the θ−2θ scans, by varying the angle of incidence θ, a diffraction pattern is recorded. The position and the intensity of the peaks are used for identifying the phase formation through their respective characteristic reflections. The ω scans are taken to check for a preferential film orientation normal to the substrate plane. In that case a strong peak from the θ−2θ scan is chosen, the detector is set and fixed to the corresponding value of the 2θ angle, as it is discussed in the next section. In this work, the crystallization of the films is studied by both, θ−2θ and ω scans. In a Bragg-Brentano geometry [54], YBCO films containing randomly oriented crystallites are identified by strong (103) reflections. Whereas YBCO films containing *a-b* and *c* oriented crystallites are recognized by high (005) and (200) reflections, respectively.

Figure 6 shows the X-ray diffractograms XRD, in semi-logarithmical scale, of the films grown on the three different substrates (LaAlO$_3$, SrTiO$_3$ and YSZ) obtained after annealing at 820, 840 and 860 °C. In all the cases, the strongest reflections are those (*h*00) corresponding to the substrate: (100), (200) and (300). Regarding the diffractions corresponding to YBCO, all the diffractograms present (00 ℓ) reflections: (002), (003), (00,4), (005), (006), and (007) indicating epitaxial growth of the film in the *c*-direction. Note that comparing to the samples annealed at 820 and 840 °C, the samples annealed at 860 °C present the highest (00 ℓ) reflections. Moreover, some (0*k*0) reflections, such as (010) and (020) are also detected, especially in the
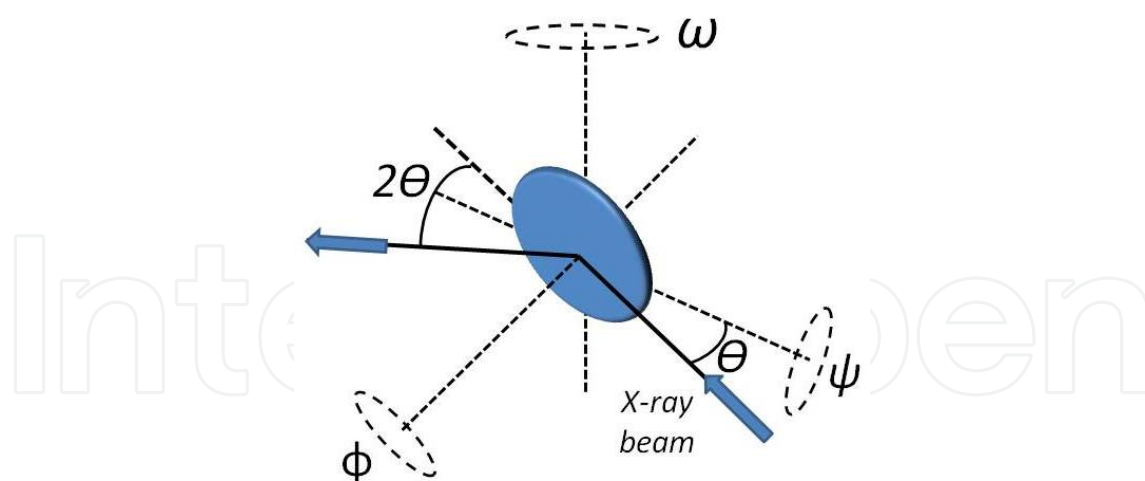
Figure 5. Four representative angles (θ−2θ, ω, ϕ and Ψ) of the goniometer in a typical diffractometer. In the θ−2θ scans, by varying the angle of incidence θ, a diffraction pattern is recorded. Whereas, the ω scans is performed over a strong peak from the θ−2θ scan. In this work, the crystallization of the films is studied by both, classical 2θ and ω scans.

diffractogram corresponding to the sample deposited on $LaAlO_3$, revealing that some crystallites grow in the *b*-direction.

On the other hand, since YBCO is a multi-cationic material, during the heat treatment at high temperatures the oxygen atoms can diffuse as they are weakly bounded to the structure, especially the oxygen atoms in the basal plane. Thus, in addition to the YBCO phase, other different stable phases can be formed according to the phase diagram. The stabilization in other structures depends on the number and arrangement of the vacant-sites of oxygen (tetrahedral or octahedral). Following the phase diagram of YBCO at 800 ℃ [55], these phases can be classified as: i) stable ($YBa_2Cu_3O_7$, $YBa_2Cu_4O_8$), ii) Secondary ($BaCuO_2$, $Y_2Cu_2O_5$, Y_2BaCuO_5, $BaCO_3$ etc), iii) unreacted (CuO, BaO, $BaCO_3$ and Y_2O_3) and iv) unstable ($BaCu_2O_2$, $Ba_2Cu_3O_{6-x}$). In the XRD presented in the figure, small reflections corresponding to the phases Y_2BaCuO_5 (Y211), Y_2O_3, $BaCuO_2$ and Cu_2BaO_2 were also detected. They are listed in Table 3. Note that in this work, no $BaCO_3$ has been detected on the XRD of the samples, indicating that the pyrolisis at 860 °C and slow rate (1 °C/min) is effective to prevent the formation of this unwanted phase. In contrast, reflections belonging to Y211 (also called 'green phase') were detected in the XRD for all the samples, suggesting that this phase might be formed during melting of the YBCO phase [56]. Y211 also acts as flux pinning centres improving the electrical and magnetic properties of the YBCO film [57]. Furthermore, the samples annealed at 820 °C present the majority amount of unreacted phases, indicating that this annealing temperature is not high enough to complete all the reaction. Besides, the less formation of secondary phases is obtained on the $LaAlO_3$ substrate while the sample containing more secondary phases is obtained on YSZ substrates. The latest suggests that as smaller is the mismatch in lattice constant to that of YBCO, there is better reaction between the coating components to form more pure YBCO. The presence of these unwanted phases affect the magnetic properties of the material, as we discuss in more detail below.
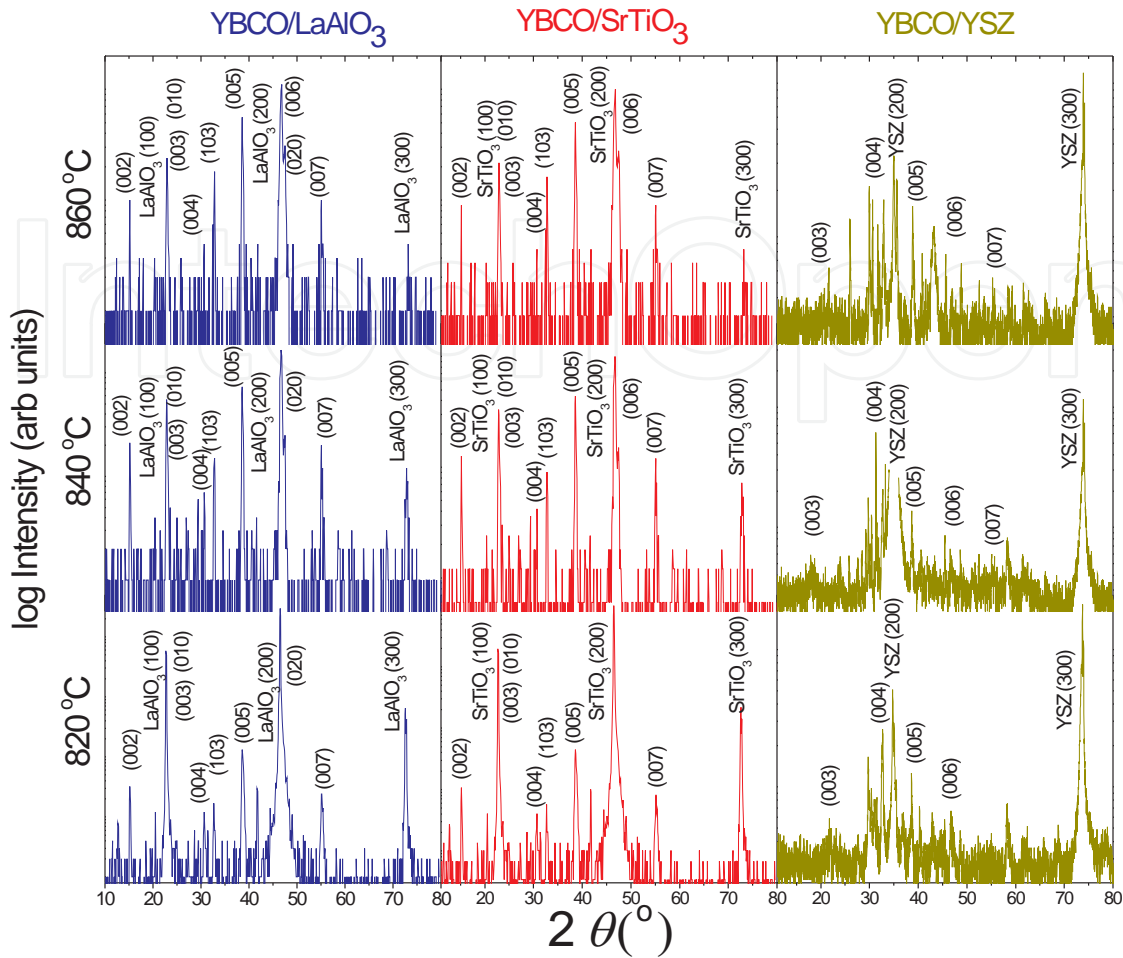
Figure 6. X ray diffractogram of YBCO films on LaAlO$_3$, SrTiO$_3$ and YSZ substrates obtained by the oxalate CSD route and annealing at 820, 840 and 860 °C. For all the cases, the strongest reflections are those (*h*00) corresponding to the respective substrates. The presence of the (00 ℓ) reflections corresponding to YBCO indicate crystallite growth in the *c*-direction. Some (0*k*0) reflections are also detected, especially in the diffractogram corresponding to the sample deposited on LaAlO$_3$, revealing that some crystallites grow in the *b*-direction.

For all the samples, the mean crystallite sizes and degree of epitaxy (f_c) for YBCO were calculated from the reflection (005) around 38.51°. The crystallite sizes were calculated with Scherrer's formula, neglecting peak broadening caused by residual stresses in the films [54]:

$$D = \frac{0.916\lambda}{\beta_{\text{hkl}}\cos\theta_{hkl}} \qquad (6)$$

where D is the average crystallite size, λ is the wavelength of the applied X-ray ($\lambda_{\text{Cu-K}\alpha 1}$=0.154056 nm), θ_{hkl} is the Bragg's angle and β_{hkl} is the pure diffraction line broadening (in radians), which were easily found by measuring the full width at the half maximum (FWHM) of the reflection. The obtained values are listed in Table 3. Note that for all the samples, the crystallite size increases with temperature and the largest grains are obtained on the sample grown in YSZ substrates and annealed at 860 °C.

To calculate f_c, the (005) and (002) intensities ($I^{(005)}$ and $I^{(002)}$ respectively) were compared to those ones provided in the PDF-2 card 89-6049 ($I_{stand}^{(005)}$ and $I_{stand}^{(002)}$ respectively) [58], following the relation:

$$\frac{I^{005}}{I^{200}} = \frac{f_c \cdot I_{stand}^{005}}{(1 - f_c) I_{stand}^{200}}$$ (7)

The f_c values are also listed in Table 3. Similar to the grain growth, f_c increases with annealing temperature, except for the samples grown on YSZ substrates. The highest f_c is also obtained on the sample grown on YSZ and annealed at 860 °C which is correlated with crystallite size and sharpest (005) reflections.

Overall, the increase of grain size and f_c values with annealing temperature observed in this work indicate that annealing promotes the epitaxial growth of the crystals orientated to (005) thus improving the crystallization of the CSD YBCO films, specially at higher temperatures.

Substrate	Annealing Temperature (°C)	Secondary Phases	Crystallite size (nm)	f_c
LaAlO₃	820	Y211, Y₂O₃, BaCuO₂,	25	0.60
	840	Y211, Y₂O₃	32	0.74
	860	Y211	33	0.88
SrTiO₃	820	Y211, Y₂O₃, BaCuO₂, Cu₂BaO₂	25	0.02
	840	Y211, Y₂O₃, BaCuO₂, Cu₂BaO₂	30	0.61
	860	Y211	35	0.64
YSZ	820	Y211, Y₂O₃, CuO, BaCuO₂	34	0.90
	840	Y211, Y₂O₃, CuO, BaCuO₂	36	0.86
	860	Y211, Y₂O₃, BaCuO₂	56	0.91

Table 3. Secondary phases, grain size and f_c values obtained from the (005) reflections from XRD of YBCO films grown in LaAlO₃, SrTiO₃ and YSZ substrates by CSD and annealing.

8. Texture

As mentioned in the previous section, X-ray diffraction can also provide qualitative information about the texture of the YBCO films. Figure 7 shows a schematic representation of inclined crystallites and their correspondent identification by ω-scans. The inclination (Fig. 7 (a)) is related to the out-of-plane deviation of the crystallites and it is also called out-of-plane texture (along the z axis). The ω– scans, also called rocking curves (Fig. 7 (b)), are obtained by scanning the ω angle as indicated in Fig. 5 above and the degree of out-of-plane texture is then deter-

mined by the FWHM value of the profile. If the rocking curve is the superposition of more than one profile, the components indicate different internal layers.
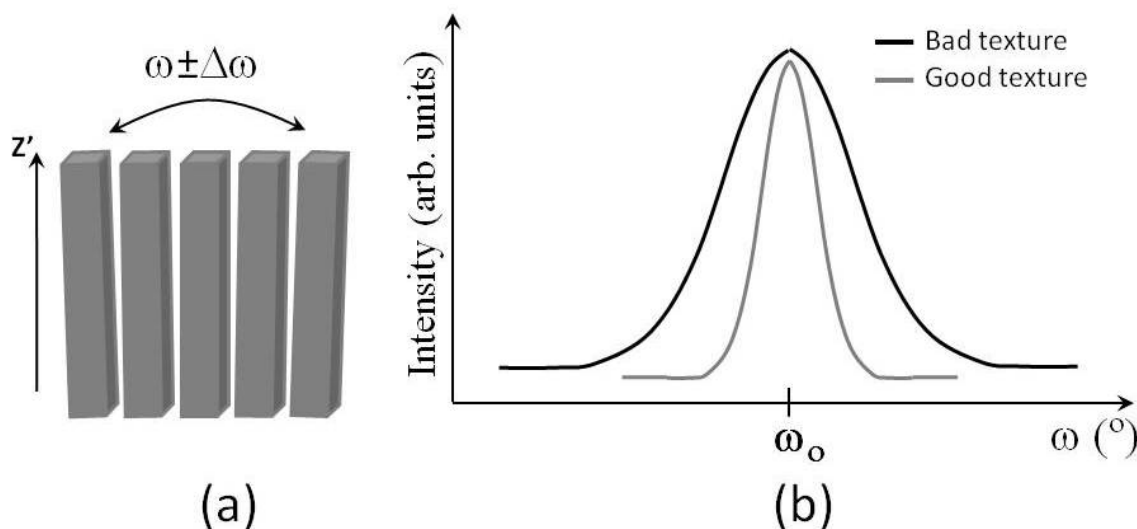

Figure 7. Schematic representation of: a) inclined crystallites and b) the correspondent identification by ω-scans by XRD.

Figure 8 shows the rocking curves corresponding to the (005) reflection of the YBCO films obtained by the oxalate CSD route on LaAlO$_3$, SrTiO$_3$ and YSZ substrates and after oxygenation at 860 °C. This reflection was chosen because its intensity is higher than the other (00ℓ) reflections and also because its position in the XRD plot (around $2\theta = 38.72°$) is far away from any other reflection (see Fig 6). As mentioned above, the values of the FWHM ($\Delta\omega$) of the rocking curves represent the degree of inclination of the crystallites with respect to the normal of the plane substrate. The rocking curves corresponding to the sample deposited on LaAlO$_3$ can be fitted with two Gaussian functions, while the samples deposited on SrTiO$_3$ and YSZ can be fitted up to three Gaussian functions respectively. Each Gaussian function provide different $\Delta\omega$ values meaning that the films consist on multilayers of YBCO of different texture. The $\Delta\omega$ values are listed in Table 4. Since the texture of the films is strongly influenced by the substrate, the smaller $\Delta\omega$ values in each sample should correspond to layers close to the YBCO/substrate interface, whereas high $\Delta\omega$ values represent textures of layers close to the film surface. Note that the sample deposited on LaAlO$_3$ present only two layers with different texture although the inner layer presents the poorest texture (with $\Delta\omega = 0.45°$) compared to those from the other samples. Despite the YBCO film deposited on SrTiO$_3$ contains three layers with different texture, the inner layer presents a better texture ($\Delta\omega = 0.35°$) than the other samples. On the other hand, the relative high lattice mismatch between YBCO and YSZ (see Table 2) was expected to influence the texture of the deposited YBCO. In fact, the intermediate and outter-layers composing it are highly distorted ($\Delta\omega = 6°$ and $9°$ respectively) although the texture of the deepest layer is similar to the other samples. The effect of increasing $\Delta\omega$ from bottom to top layers is characteristic of films increasing in thickness, once a critical or threshold thickness is exceeded, the out-of-plane texture becomes negative.
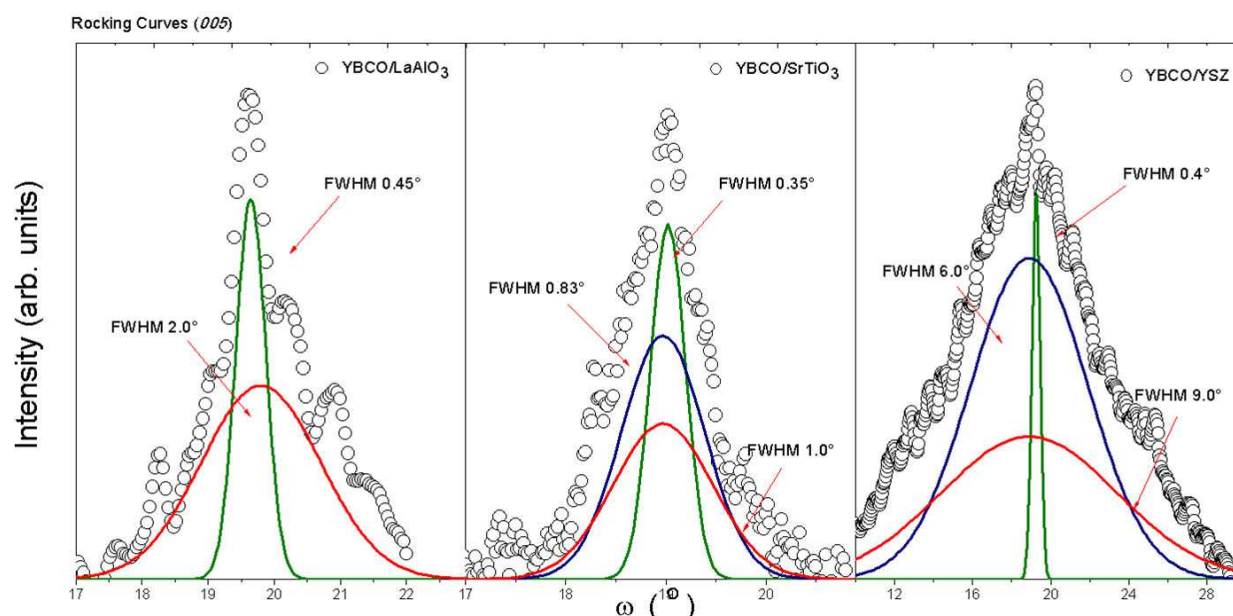
Rocking Curves (*005*)

Figure 8. Rocking curves corresponding to the (005) reflection of the YBCO films obtained by CSD on LaAlO$_3$, SrTiO$_3$ and YSZ substrates, after oxygenation at 860 °C. The rocking curves corresponding to the sample deposited on LaAlO$_3$ can be fitted with two Gaussian functions, while the samples deposited on SrTiO$_3$ and YSZ can be fitted up to three Gaussian functions respectively. Each Gaussian function provides a different $\Delta\omega$ value which is listed in Table 4.

Position	LaAlO$_3$	SrTiO$_3$	YSZ
Close to the film/substrate interface	0.45°	0.35°	0.4°
Intermediate layer	-	0.83°	6.0°
Close to the surface	2.0°	1.0°	9.0°

Table 4. Full width at the half maximums (FWHM, $\Delta\omega$) of the rocking curves corresponding to the reflection (005) for YBCO films obtained by the oxalate CSD route on LaAlO$_3$, SrTiO$_3$ and YSZ substrates and after oxygenation at 860 °C.

9. Superconductivity

Figure 9 shows the magnetic moment vs. temperature of the YBCO films on LaAlO$_3$, SrTiO$_3$ and YSZ substrates obtained by the oxalate CSD route and oxygenation at 860 °C. The plots show the measurements taken in zero field cooling (ZFC) and field cooling (FC) modes for external magnetic field applied parallel to the film plane of 100 mT for films deposited on LaAlO$_3$ and SrTiO$_3$ and 50 mT for that deposited on YSZ. The superconducting property of the obtained films is demonstrated by the diamagnetic signals below the transition temperature T$_C$=90 K, thus confirming the formation of the superconducting YBCO. Note that the sample deposited on YSZ shows an up turn in the diamagnetic signal at low temperature, which can be attributed to other phases which are present in the sample. In fact, according to Table 3, this sample contains more secondary and unreacted phases than the other samples oxygenated at

860 °C. Therefore, the diamagnetic behaviour of the YBCO superconductor is screened by the paramagnetic response of those unwanted phases. The latest is better distinguished at the lowest temperatures in which the paramagnetic response tends to rise both, the ZFC and FC, branches to positive values of the magnetic moment.
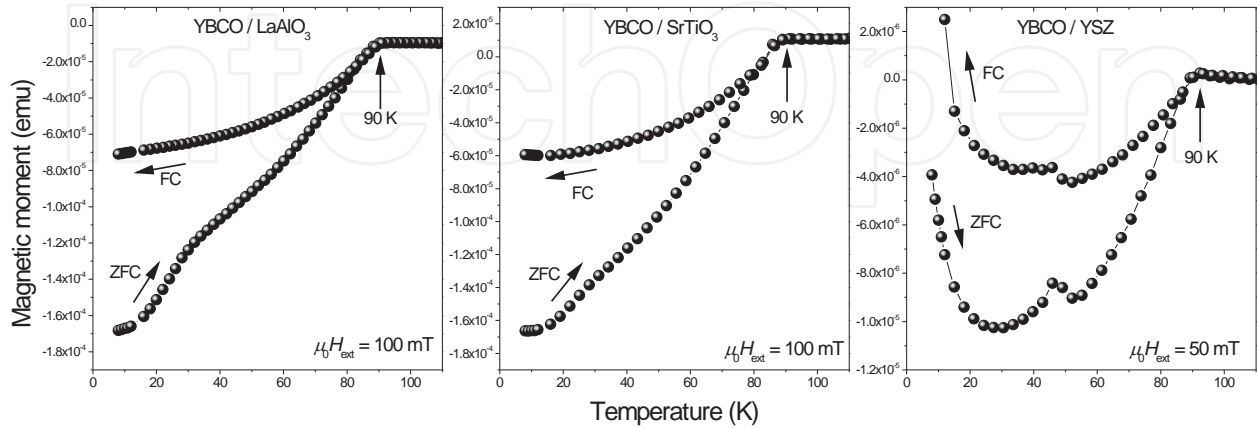

Figure 9. Magnetic moment vs. temperature of YBCO films on LaAlO$_3$, SrTiO$_3$ and YSZ substrates obtained by oxalate CSD and oxygenation at 860 °C. The magnetic measurements were taken in zero field cooling (ZFC) and field cooling (FC) modes. The superconducting property is demonstrated by the diamagnetic signals below the transition temperature 90 K. The samples deposited on LaAlO$_3$ and SrTiO$_3$ were measured under $\mu_0 H_{ext}$=100 mT while the sample deposited on YSZ was measured under $\mu_0 H_{ext}$=50 mT.

10. Conclusions

YBa$_2$Cu$_3$O$_7$ films were successfully deposited on LaAlO$_3$, SrTiO$_3$ and YSZ by the oxalate CSD route and heat treatments at 820, 840 and 860 °C. The preparation of the precursor solution does not require trifluoroacetates components. The obtained samples consist of granular YBCO films. X-ray diffraction reveals that all the samples contain crystallites oriented to (00 ℓ) indicating epitaxial growth of the film in the c-direction. Remarkably, similar to the trifluoroacetates CSD route, the oxalate route presented here does not form BaCO$_3$. However, small amounts of other phases, such as Y$_2$BaCuO$_5$ (Y211), Y$_2$O$_3$, BaCuO$_2$ and Cu$_2$BaO$_2$, were formed. The grain size and the degree of crystallinity values increase with annealing temperature leading in more epitaxial and pure YBCO films. Thus, the samples oxygenated at 860 °C present less unreacted and secondary phases, and higher (00 ℓ) reflections than the sample oxygenated at 820 and 840 °C. Rocking curves corresponding to the (005) reflection of these films can be fitted with more than one Gaussian functions meaning that they consist on multilayers of YBCO with different texture. Moreover, the relative high lattice mismatch between YBCO and YSZ was reflected in the texture of the corresponding grown YBCO layer. The superconducting property of the obtained films is demonstrated by their corresponding magnetic measurements confirming the formation of the superconducting YBCO with T$_C$=90 K. However, for the case of the sample deposited on YSZ its corresponding diamagnetic signal is distorted by the paramagnetic responses of the unwanted phases within this sample.

Acknowledgements

Author details

Luis De Los Santos Valladares[1*], Juan Carlos González[2], Angel Bustamante Domínguez[2], Ana Maria Osorio Anaya[3], Henry Sanchez Cornejo[2], Stuart Holmes[1], J. Albino Aguiar[4,5] and Crispin H.W. Barnes[1]

*Address all correspondence to: luisitodv@yahoo.es

1 Cavendish Laboratory, Department of Physics, University of Cambridge, J.J. Thomson Ave., Cambridge, United Kingdom.

2 Laboratorio de Cerámicos y Nanomateriales, Facultad de Ciencias Físicas, Universidad Nacional Mayor de San Marcos, Lima, Peru

3 Facultad de Química e Ingeniería Química, Universidad Nacional Mayor de San Marcos, Ciudad Universitaria, Lima, Peru

4 Departamento de Física, Universidade Federal de Pernambuco, Recife, Brazil

5 Programa de Pós-Graduação em Ciência de Materiais, Centro de Ciências Exatas e da Natureza, Universidade Federal de Pernambuco, Recife, Brazil

References

[1] G. Desgardin, I. Monot y B. Raveau, Supercond. Sci. Technol. 12 (1999) R115.

[2] E. K. Hollmannt, O. G. Vendik, A. G. Zaitsev y B.T. Melekh, Supercond. Sci. Technol. 7 (1994) 609.

[3] J. L. Mayo, Superconductivity: The Threshold of a New Technology, TAB Books, Inc., Blue Ridge Summit, Pasadena (1989).

[4] W. A. Harrison, Phys. Rev. B 38 (1988) 270.

[5] C. Poole, H.A. Farach, R.J. Creswick, R. Prozorov, Superconductivity, 2nd ed., Academic Pres, The Netherlands 2007.

[6] High performance YBCO-coated superconductors wires, MRS Bulletin 29 No 8 (2004).

[7] S. U. K. Nair, P. R. S. Warriary J. Koshy; Bull. Mater. Sci. 25, (2002) 95.

[8] D. P. Norton; Annu. Rev. Matter. Sci. 28, 299 (1998).

[9] R. Wondenweber, Supercond. Sci. Technol. 12 (1998).

[10] T. Manabe, I. Yamaguchi, S. Nakamura, W. Kondo, T. Kumagai, S. Mizuta, J. Mat. Res. 10 (1995) 1635-1643.

[11] J.A. Smith, M.J. Cima, N. Sonnenberg, IEEE Trans. Appl. Supercond. 9 (1999)1531-1534.

[12] K. Yamagiwa, T. Araki, Y. Takahashi, H. Hier, S.B. Kim, K. Matsumoto, J. Shibata, T. Hirayama, H. Ikuta, U. Mizutani, I. Hirabayashi, J. Crystal Growth 229 (2001) 353-357.

[13] T. Araki, I. Hirabayashi, Supercond. Sci. Techn. 16 (2003) R71-R94.

[14] K. Yamagiwa, T. Araki, Y. Takahashi, H. Hiei, S. B. Kim, K. Matsumoto, J. Shibata, T. Hirayama, H. Ikuta, U. Mizutani, I. Hirabayashi; J. Cryst. Growth 229, 353 (2001).

[15] O. Castano, A. Cavallaro, A. Palau, J. C. Gonzalez, M. Rossell, T. Puig, F. Sandiumenge, N. Mestres, S. Pinol, A. Pomar, X. Obradors; Supercond. Sci. Technol. 16, 45-53 (2003).

[16] R.W. Schwartz, Chem. Mater, 9 (1997) 2325-2340.

[17] W. Cui, J.L. Tanner, T.W. Button, J. Phys.: Conf. Series, 97 (2008) 012257.

[18] K. Knoth, S. Egel, C. Apettri, M. Falter, B. Schlobach, R. Huhne, S. Oswald, L. Schultz, B. Holzapfel, Current Op. Sold. Stat. Mat. Sci., 10 (2006) 205-216.

[19] A. Sheth, K. Trembath, J. Mat. Process. Tech., 123 (2002) 167-178.

[20] M.E. Gross, M. Hong, S.H. Liou, P.K. Gallagher, J. Kwo, Appl. Phys. Lett. 52 (1988) 160-162.

[21] M.L. Kullberg, M.T. Lanagan, W. Wu, R.B. Poeppel, Supercond. Sci. Technol. 4 (1989) 337-342.

[22] Y.L. Chen, J.V. Mantese, A.H. Hamdi, A.L. Mecheli, J. Mater. REs. 4 (1989) 1065-1070.

[23] K. Yamagiwa, H. Hiei, Y. Takahashi, S.B. Kim, K. Matsumoto, H. Ikuta, U. Mizutani, I. Hirabayashi, Physica C 334 (2000) 301-305.

[24] P.C. McIntyre, M.J. Cima, J.A. Smith, R.B. Hallock, M.P. Siegal, J.M. Phillips, J. Appl. Phys. 71 (1992) 1868-1877.

[25] P.C. McIntyre, M.J Cima, A. Roshko, J. Appl. Phys. 77 (1995) 5263-5272; S. Sathya-murthy, K. Salama, Physica C 329 (2000) 58-68.

[26] A. Malozemoff, S. Annavarapu, L. Fritzmeier, Q. Li, V. Prunier, M. Rupich, C. Thieme, W. Zhang, A. Goyal, M. Paranthaman, D.F. Lee, Supercond. Sci. Technol. 13 (2000) 473-476.

[27] A. Gupta, R. Jagannathan, E.I. Cooper, E.A. Giess, J.I. Landman, B.W. Hussey, Appl. Phys. Lett. 52 (1988) 2077-2079.

[28] P.C. McIntyre, M.J. Cima, J.A. Smith, R.B. Hallock, M.P. Siegal, J.M. Phillips, J. Appl. Phys., 71 (1992) 1868-1877.

[29] X.M. Cui, B.W. Tao, Z. Tian, J. Xiong, X.Z. Liu, Y.R. Li, Supercond. Sci. Technol. 19 (2006) L13-L15.

[30] S. Wang, L. Wang, B. Gu, J. Mater. Sci. Technol. 24 (2008) 899-902.

[31] X. Tang, Development of a fluorine-free chemical solution deposition route for rare-earth cuprate superconducting tapes and its application to reel-to-reel processing, PhD Thesis, Technical University of Denmark, Denmark, 2013.

[32] I.H. Mutlu, H. Acun, E. Celick, H. Turkmen, Physica C 451 (2007) 98-106.

[33] K.S. Mazdiyashi, C.T. Lynch, J.S. Smith, Inorg. Chem., 5 (1996) 342-346.

[34] B. Zhao, H.B. Yao, K. Shi, Z.H. Han, Y.L. Xu, D.L. Shi, Physica C 386 (2003) 348-352.

[35] J. Lian, H. Yao, D. Shi, L. Wang, Y. Xu, Q. Liu, Z. Han, Supercond. Sci. Technol. 16 (2003) 838-844.

[36] S. Shi, Y. Xu, H. Yao, Z. Han, J. Lian, L. Wang, A. Li, H.K. Liu, S.X. Dou, Supercond. Sci. Tech. 17 (2004) 1420-1425.

[37] Q.X. Jia, T.M. McCleskey, A.K. Burrell, Y. Lin, G.E. Collis, H. Wang, A.DQ. Li, S.R. Foltyn, Nature Matt. 3 (2004) 529.

[38] T. Manabe, I. Yamaguchi, H. Obara, S. Kosaka, H. Yamasaki, M. Sohma, T. Tsuchiya, S. Mizuta, T. Kumagai, Physica C 378-381 (2002) 1017-1023.

[39] D. Shi, Y. Xu, S.X. Wang, J. Lian, L.M. Wang, S.M. Mc Clellan, R. Buchanan, K.C. Goretta, Physica C 371 (2002) 97-103

[40] A.H. Li, M. Ionescu, H.K. Liu, D.L. Shi, X.L. Wang, X. Peng, E.W. Collings, Physica C 426-431 (2005) 1408-1414.

[41] H. Yao, B. Zhao, K. Shi, Z. Han, Y. Xu, D. Shi, S. Wang, L.M. Wang, C. Peroz, C. Villard, Physica C 392-396 (2003) 941-945.

[42] L. Lei, G.Y. Zhao, J.J. Zhao, H. Xu, IEEE Trans. Appl. Supercond. 20 (2010) 2286-2293.

[43] C. Apetrii, H. Schlorb, M. Falter, I. Lampe, L. Schultz, B. Holzapfel, IEEE Trans. Appl. Supercond. 15 (2005) 2642-2644.

[44] A. Bustamante Domínguez, A. M. Osorio, L. De Los Santos Valladares, H. Carhuancho, J.C. González, G.R.C. Cernicchiario, J.A. Feijoo Lévano, Advances in Science and Technology 47 (2006) 37-42.

[45] H.E. Sanchez, A. Bustamante Domínguez, A. Osorio Anaya, L. De Los Santos Valladares, J. Albino Aguiar, C.H.W. Barnes, J. Chem. Chem. Eng. 8 (2014) 547-511.

[46] A. Bustamante Domínguez, A.M. Osorio, L. De los Santos Valladares, J. Garcia, J.C. González, C.H.W. Barnes, Y. Azuma, Y. Majima, J. Albino Aguiar, J. Phys.: Conf. Ser. 507 (2014) 01005.

[47] A. Bustamante Domínguez, L. León Felix, J. Garcia, J. Flores Santibañez, L. De Los Santos Valladares, J.C. González, A. Osorio Anaya, M. Pillaca, Phys. Proc. 36 (2012) 526-531.

[48] J. García, A. Bustamante Domínguez, L. De Los Santos Valladares, J.C. González, L. León Felix, J. Flores Santibañez, A. Osorio Anaya, J. Albino Aguiar, Rev. Inv. Fis. 15 (2012) 121502102 (in Spanish).

[49] J.C. González, A. Osorio, A. Bustamante, Rev. Soc. Quim. Peru 77 (2011) 249 (in Spanish).

[50] J. Jorgensen, M. Beno, D. Hinks, L. Sodeholm, K. Volin, C. Segre, K. Zhang, M. Kleefisch, Phys. Rev. B 36 (1987) 3608.

[51] Z. Aslanoglu, Y. Akin, M.I. El-Kawni, W. Sigmund, Y.S. Hascicek, Physica C 384 (2003) 501-506.

[52] A. Bustamante Domínguez, L. De Los Santos Valladares, J. Flores Santibañez, R. Lozano, J. Palomino, G.R.C. Cernicchiario, Rev. Inv. Fis. 7 (2004) 30-33.

[53] J.C. González, L. De Los Santos Valladares, A.M. Osorio Anaya, J. Albino Aguiar, A. Bustamante Domínguez, Rev. Inv. Fis. 15 (2012) 121501104 (in Spanish).

[54] B. D. Cullity, Elements of X-ray Diffraction (Addison-Wesley Publishing Company, Inc. USA, 1956), pp.96-102.

[55] E. Brosha, F. Garzon, I. Raistrick, P. Davies, J. Am. Ceram. Soc. 78 (1995) 1745.

[56] M. Llosa, L. de los Santos Valladares, N. de la Cruz Centeno, A. Bustamante Domínguez, Rev. Inv. Fis. 7 (2004) 34-37 (in Spanish).

[57] F. Frangi, T. Higuchi, M. Deguchi, M. Murakmi, J. Matter. Res. 10 (1995) 2241-2250.

[58] Powder Diffraction Files PDF-2 of The International Centre for Diffraction Data® (ICDD®)-2001.